RUL Prediction of Lithium-ion Batteries Based on TimeGAN-Pyraformer-BiLSTM

Xiaoxin Li, *Member, IAENG,* Qiang Ai*, *Member, IAENG,* Ming Xu

***Abstract*—The capacity of lithium-ion batteries gradually degrades over time, presenting unforeseen risks and losses. Models based on data-driven approaches and neural network predictions can offer early warnings for battery failure. However, common models often face challenges with error accumulation in predicting future capacity changes, and insufficient data complicates model training. To address this, a novel method for predicting remaining battery life is proposed. This method incorporates IC analysis, DTV analysis, and Local Linear Embedding algorithms for efficient feature extraction and uses TimeGAN to augment training data, creating an integrated prediction framework. It combines the long-sequence prediction capabilities of the Pyraformer network with the dynamic multi-variable relationship capturing of the BiLSTM network, enhancing the model's understanding of capacity degradation trends. Comparative experiments demonstrate that this approach achieves higher prediction accuracy than traditional simple neural networks. Additionally, ablation studies further confirm the effectiveness of the introduced techniques in prediction tasks.**

***Index Terms*—Lithium-ion battery, capacity degradation model, data augmentation, Pyraformer network, time series prediction.**

I. Introduction

GIVEN the escalating concerns over environmental degradation, electric vehicles (EVs) are increasingly becoming the preferred mode of transport. The power battery, serving as the heart of EVs, is pivotal to their performance. Among the diverse battery technologies, lithium-ion batteries stand out as the predominant choice due to their superior benefits [1]. Nonetheless, these batteries undergo progressive aging during their lifecycle, characterized by rising internal resistance and diminishing capacity, adversely impacting battery performance [2]–[4]. Notably, the likelihood of thermal runaway and related safety hazards escalates markedly when battery capacity falls below 80% of its original value, indicating the nearing end of its service life [5]–[7]. Consequently, precise estimation of a battery's remaining useful life (RUL) is crucial for optimizing battery utilization and ensuring safety [3]. This endeavor is notably complex and vital, as the RUL is influenced by various factors, including internal chemical reactions, the operational environment, and usage patterns [5]. Present strategies for RUL estimation of batteries primarily encompass model-based and data-driven methodologies [8]–[11].

Manuscript received March 13, 2024; revised July 8, 2024.

Xiaoxin Li is a postgraduate student at the Software College, Liaoning Technical University, Huludao, Liaoning, 125105, China (phone: +8613358819070; e-mail: lixiaoxin1999@aliyun.com).

Qiang Ai is a postgraduate student at the School of Computer, Qinghai Normal University, Xining, Qinghai, 810008, China (corresponding author to provide phone: +8617813140425; e-mail: qiang.ai@outlook.com).

Ming Xu is a professor at the Software College, Liaoning Technical University, Huludao, Liaoning, 125105, China (phone: +8615810261581; e-mail: xum.2016@tsinghua.org.cn).

Model-based forecasting typically involves the development of mathematical or physical models to elucidate the degradation mechanisms of lithium-ion batteries, focusing on the internal physicochemical processes, such as formulating Equivalent Circuit Models (ECMs) and electrochemical models for RUL estimation. Research [12] delves into the internal dynamics of lithium-ion batteries through electrochemical modeling to predict RUL. Nonetheless, crafting precise models poses challenges due to the dynamic and nonlinear nature of electrochemical reactions. The complexity in developing an ECM lies in accurately replicating the battery's electrochemical behavior and choosing the right circuit elements and parameters that mirror actual battery performance [13]. Furthermore, research [14] integrates particle filtering (PF) with empirical mode decomposition (EMD) for end-of-life estimation, streamlining the PF parameter adjustment process and employing EMD for state estimation to prevent overfitting. Research [15] introduces a semi-empirical approach that leverages battery charge/discharge cycles for swift and precise RUL predictions. Research [16] enhances ECM accuracy by incorporating sensor bias and employs an adaptive variable structure filter with a variable boundary layer approach for battery state of health (SOH) estimation through internal resistance measurement. Research [17] links battery aging to phenomena like cathode agglomerate fragmentation and changes in anode solid electrolyte interface (SEI) film thickness, proposing a comprehensive cell impedance model for RUL estimation by examining SOH-related parameters. Conversely, research [18] adopts an advanced dual-polarization technique for ECM development. While model-based methods, particularly ECM and electrochemical modeling, offer precise predictions, they encounter applicability challenges due to varying performances across different battery types and operational conditions. The intricate mechanisms and multifactorial interactions complicating battery usage also make high-accuracy model construction difficult. Moreover, the precision of RUL predictions heavily relies on model parameter configurations, highlighting the challenges and limitations in establishing accurate degradation prediction models.

In contrast to the model-based methodology, data-driven strategies bypass the need for an in-depth understanding of lithium batteries' internal mechanisms. Instead, they focus on uncovering the underlying patterns of battery degradation through the analysis of historical operational data to forecast the remaining useful life (RUL). Data-driven approaches, particularly through deep learning techniques, excel in feature extraction, nonlinear mapping, and adaptability. These include the use of deep belief networks (DBN) [19], residual networks (ResNet) [20], and various forms of recurrent neural networks (RNN) [21], with gated recurrent units (GRU) [22] and long short-term memory networks (LSTM)

[23] being notably prevalent. Nonetheless, traditional RNNs are prone to issues like the vanishing and exploding gradient problems, making it challenging to maintain long-term dependencies [24]. Furthermore, GRUs and LSTMs can struggle with the retention of sequence and historical information, particularly when processing very long time series, potentially leading to information loss and dilution.

Addressing the challenge of capturing long-term dependencies, the team at Google introduced the Transformer model [25], leveraging an attention mechanism designed to efficiently process sequential temporal information and excel in identifying long-range relationships. Building upon this foundation, research [26] introduced the Pyraformer, a novel model characterized by its pyramidal attention mechanism tailored for time series analysis and forecasting. The Pyraformer distinguishes itself from the Transformer by employing a multi-resolution strategy to analyze temporal dependencies across various scales, enabling it to grasp extended temporal correlations with comparable computational efficiency. Unlike recursive models like RNNs, which cannot be executed in parallel, and convolutional models such as CNNs, which, despite being parallelizable, suffer from high parameter counts and computational demands, Transformers and their derivatives like the Pyraformer excel in parallel processing. The Pyraformer not only retains the parallel processing capabilities of the Transformer but also enhances the model's proficiency in managing long-range temporal relationships through its innovative architecture, offering distinct advantages in temporal data analysis and prediction tasks.

In the realm of data-driven approaches for predicting the remaining useful life (RUL) of batteries, identifying Health Indicators (HI) plays a crucial role. However, while battery capacity and resistance are frequently used as direct indicators for RUL estimation, their measurement is not feasible in real-time and requires specialized equipment in a controlled laboratory setting [27], [28]. Data-driven techniques primarily rely on regression analysis of pertinent performance metrics, making the selection of a health indicator that precisely mirrors battery wear and tear especially significant.

In the analysis of battery degradation, relying on a singular feature often fails to capture the complete aging patterns. Utilizing a combination of features can address this limitation, thereby improving the predictive model's accuracy. Research [29] introduced an enhanced technique for deriving Incremental Capacity (IC) curves by gathering IC curves through reference voltages and identifying incremental capacity values over various voltage ranges as features. Research [30] employed segments of charging curves for IC analysis, selecting pertinent curves for feature extraction. Research [31] identified critical points and deviations as features of thermo-electric coupling through analyses like IC, Differential Thermal Voltage (DTV), and Differential Thermal Capacity (DTC), integrating these with internal resistance to enrich the model's input features. Although diverse approaches exist for feature extraction, the relevance and applicability of these features can vary significantly across different battery systems and operational scenarios. The combined use of multiple features helps overcome the limitations of single-feature data representation, but the significance of each feature can differ across time series. This variation poses a challenge for deep learning models, which may struggle to prioritize the most relevant features, potentially leading to underutilization of critical feature information. Furthermore, the process of selecting multiple features is complex, necessitating a balance between relevance to battery aging, computational efficiency, and the avoidance of unnecessary complexity and redundant data.

Data-driven methodologies encounter several obstacles, including the challenges of limited training datasets, uneven data distribution, and noisy data. Research [32] introduced a strategy utilizing Auxiliary Classifier Generative Adversarial Networks (ACGAN) to effectively address the issue of imbalanced fault data, thereby enhancing the diagnostic accuracy and generalizability. Nonetheless, when it comes to processing battery-related data, traditional Generative Adversarial Networks (GANs), Conditional GANs (CGANs), and ACGANs face significant hurdles [33], [34]. These include struggles with capturing the variability in battery data, inadequacies in managing uneven data distributions, and difficulties in replicating complex noise patterns and evolving data distributions. Consequently, this study adopts TimeGAN (Time-Conditional Generative Adversarial Networks) [35], specifically designed for addressing multivariate time series challenges, as a strategy for data augmentation.

This study introduces a novel approach for predicting the remaining useful life (RUL) of lithium-ion batteries, utilizing a combination of TimeGAN, Pyraformer, and BiLSTM technologies. The method begins with dimensionality reduction through local linear embedding, applying insights from Incremental Capacity (IC) and Differential Thermal Voltage (DTV) analyses to delineate the thermal and electrochemical shifts indicative of battery aging. TimeGAN is then employed to augment the dataset with synthetic data, mirroring the original dataset's features to increase its diversity. The core of the prediction methodology is a network that integrates Pyraformer with BiLSTM for both training and evaluation of its predictive accuracy. The Pyraformer's strength lies in its adeptness at detecting variations across multiple time scales, essential for grasping both the immediate and extended trends within time series data. It excels in pinpointing critical sequential moments, thereby enhancing feature significance and facilitating effective feature integration. The inclusion of a Bi-directional Long Short-Term Memory (BiLSTM) network amplifies this capability by examining data sequences from both directions, ensuring a thorough contextual understanding of the time series. This dual analysis aids in grasping intricate temporal relationships and forecasting forthcoming patterns. By merging the Pyraformer's robust feature detection with the BiLSTM's trend analysis refinement, this framework offers a sophisticated solution for analyzing and forecasting complex temporal data sequences.

This study performs simulation tests using battery aging data from the collaborative dataset provided by the Massachusetts Institute of Technology (MIT), Stanford University, and the Toyota Research Institute [36], as well as the lithium-ion battery degradation dataset from the University of Oxford [37]. Experimental validations are carried out on capacity degradation curves across various material systems and operating conditions to showcase the proposed method's efficacy and adaptability in predicting the remaining useful

life (RUL) of batteries. Through comparative analyses, this research confirms that the RUL prediction approach introduced herein significantly enhances prediction precision over conventional recurrent neural network (RNN) methods.

II. DATASET

A. Description Of Dataset

In this research, the battery aging dataset from the collaboration between the Massachusetts Institute of Technology (MIT), Stanford University, and the Toyota Research Institute, hereafter referred to as the Massachusetts dataset, employs a lithium iron phosphate battery system. Conversely, the lithium-ion battery degradation dataset from the University of Oxford, henceforth called the Oxford dataset, utilizes a ternary battery system. The Oxford dataset comprises eight batteries, labeled #1 through #8, among which batteries #2, #5, and #6 exhibit issues like abrupt voltage drops and are thus excluded from the experiments in this study. Consequently, batteries #1, #3, #4, #7, and #8 are chosen for the experimental analysis. From the MIT dataset, batteries numbered 20, 22, 36, and 44 are selected for investigation. The technical specifications of these batteries are detailed in Table I. Figure 1 illustrates the capacity degradation curves for the batteries examined from both datasets.

TABLE I: DETAILED BATTERY TECHNOLOGY INFORMATION.

	MIT Dataset	Oxford Dataset
Battery Model	APR18650M1A	Kokam CO LTD
Nominal Capacity	1.1Ah	740mAh
End-of-Life Capacity	0.88Ah	–
Ambient Temperature	30°C	40°C
Nominal Voltage	3.3V	3.7V

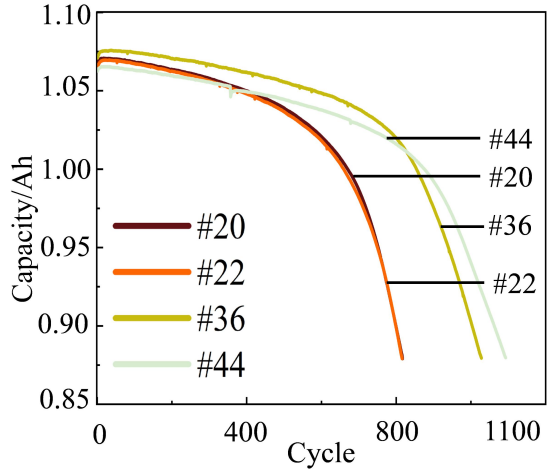

(a) MIT dataset.

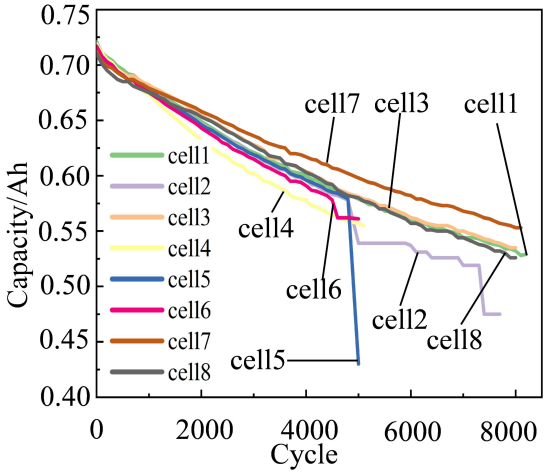

(b) Oxford dataset.

Fig. 1: Capacity degradation trajectory.

B. Feature Extraction Method

1) Feature dimensionality reduction method: Local Linear Embedding (LLE) serves as a method for reducing the dimensionality of high-dimensional data in a nonlinear fashion. It operates by identifying and preserving the data's inherent geometric structure through linear approximations within local neighborhoods, subsequently projecting the data into a space of lower dimensionality. In the process of feature extraction using LLE, data is typically organized into a matrix that denotes the neighborhood connections among data points, with each matrix element indicating the proximity between samples.

In conventional approaches, feature extraction typically focuses on identifying the peaks and valleys within DTV and IC signals. This method relies on direct signal attributes. Conversely, when employing Local Linear Embedding (LLE) for feature extraction, it doesn't directly target these peaks and valleys as features. Instead, LLE discerns the data's underlying manifold structure by establishing linear connections in local neighborhoods, thereby transitioning the data into a newly lower-dimensional representation. Through this process, LLE autonomously uncovers significant features within the data, extending beyond just the peaks and valleys.

The procedural steps of the LLE algorithm are outlined as follows.

Considering a collection of samples within a high-dimensional space: $\mathbf{X} = [\mathbf{x}_1, \mathbf{x}_2, \mathbf{x}_3, \ldots, \mathbf{x}_N]$, where $\mathbf{x}_i \in \mathbb{R}^D$, and $\mathbf{x}_i$ $(i = 1, 2, \ldots, N)$ is the ith sample, N is the total number of samples, and D is the dimensionality of the features in the high-dimensional space. Compute the Euclidean distance between each sample point and other points, as shown in Equation 1:

$$D_{ij} = \sqrt{\sum_{j=1}^{N} (x_i - x_j)^2} \tag{1}$$

The obtained Euclidean distances D_{ij} are arranged in ascending order, and the k $(k < N)$ nearest neighbors to the sample point are selected, forming the neighborhood set of x_i: $Q(i) = [x_{i1}, x_{i2}, \ldots, x_{ik}]$.

Calculate the weight matrix W, finding a linear relationship for the regression problem. For the sample X, use the mean squared error to calculate the loss function.

$$\zeta_w = \sum_{i=1}^{N} \sum_{j \in Q_i} w_{ij} (x_i - x_j)^2 \tag{2}$$

Where $Q(i)$ is the collection of k nearest neighbor samples

of i, to ensure that the sample points maintain invariance in the local neighborhood of the manifold after rotation, scaling, and translation, while also imposing a normalization constraint on the weight coefficients w_{ij}, that is, to satisfy

$$\sum_{j \in Q(i)} w_{ij} = 1 \tag{3}$$

For samples x_j that are not in the neighborhood of x_i, set the corresponding weight value $w_{ij} = 0$. Matrixize Equation (2) as follows:

$$\begin{aligned} \zeta_W &= \sum_{i=1}^{N} \left\| x_i - \sum_{j \in Q(i)} w_{ij} x_j \right\|_2^2 \\ &= \sum_{i=1}^{N} \sum_{j \in Q(i)} w_{ij} \left\| x_i - \sum_{j \in Q(i)} w_{ij} x_j \right\|_2^2 \\ &= \sum_{i=1}^{N} W_i^T (x_i - x_j)(x_i - x_j)^T W_i \end{aligned} \tag{4}$$

Where $W_i = (w_{i1}, w_{i2}, \ldots, w_{ik})^T$.

Let the matrix $Z_i = (\mathbf{x}_i - \mathbf{x}_j)(\mathbf{x}_i - \mathbf{x}_j)^T$, and obtain the weight coefficients using the Lagrange multiplier method:

$$W_i = \frac{z_i^{-1} 1_k}{1_k^T z_i^{-1} 1_k} \tag{5}$$

where 1_k is a k-dimensional all-1 column vector. Keeping this weight matrix W_i unchanged, the set of low-dimensional embeddings of the high-dimensional samples $Y_i = (y_{i1}, y_{i2}, \ldots, y_{iN})^T$ is obtained by constructing the reconstruction error function and minimizing the error. The error function is defined as follows

$$\zeta(y) = \sum_{i=1}^{N} \left\| y_i - \sum_{j=1}^{N} w_{ij} y_j \right\|_2^2 \tag{6}$$

The function needs to satisfy the restriction $\sum_{i=1}^{N} y_i = 0, \quad \frac{1}{N} \sum_{i=1}^{N} y_i y_i^T = I$. Equation 6 can be transformed into

$$\zeta(y) = \text{tr}\left(Y(I - W)(I - W)^T Y^T\right) \tag{7}$$

Let $M = (I - W)(I - W)^T$ and compute the first d smallest eigenvalues of the matrix M. Take the first $2 \sim d{+}1$ eigenvalues to obtain the low-dimensional embedding $Y_i = (y_{i1}, y_{i2}, y_{i3}, \ldots, y_{iN})^T$, $i = 2, 3, \ldots, d{+}1$, and then arrange the low-dimensional coordinates into an output matrix: $y = (y_2, y_3, \ldots, y_{d+1})^T$.

2) Incremental capacity analysis(IC):

The incremental capacity analysis method effectively connects the aging of batteries to the intercalation and de-intercalation processes of lithium ions in the electrodes. This technique visualizes the aging process by examining the correlation between changes in voltage and capacity, where the voltage plateau appears as peaks and troughs on the curve. This allows for an efficient monitoring and characterization of battery degradation. The formula for conducting incremental capacity analysis is presented as follows:

$$\frac{dQ}{dV} = I \times \frac{dt}{dV} \tag{8}$$

where Q denotes the discharge capacity, I denotes the discharge current, V denotes the discharge voltage, and t denotes the discharge time.The process of IC analysis, which involves differentiation, naturally magnifies errors originating from the data collection phase. Hence, preprocessing the data is a critical initial step in IC analysis. This preprocessing encompasses adjusting the sampling frequency and applying filtering techniques. For the dataset from Oxford, the sampling frequency was standardized to every 20 seconds. In the case of the dataset from MIT, where the sampling intervals were inconsistent, only the filtering step was implemented. The Savitzky-Golay (SG) filter was employed for its efficacy in preserving the integrity of peak and valley details within the data. The computation for the SG filter is outlined as follows:

$$y_i = \sum_{j=-p}^{j=p} \frac{1}{N_c} C_j x_{i+j} \tag{9}$$

where y denotes the smoothed signal, C_j denotes the coefficients, and x denotes the signal. Figure 2 demonstrates the changes in the DTV and IC curves as the battery ages. The peaks move with aging and the associated features are closely related to the capacity.

3) differential voltammetric analysis (DTV):

The Differential Thermal Voltage (DTV) analysis method leverages entropy variations throughout the battery's aging process as a descriptor. With aging, the battery undergoes energy and phase transitions, manifesting as alterations in entropy. Thus, the aging of batteries is assessable through the examination of both voltage and temperature indicators. The methodology for DTV analysis is summarized as follows:

$$DTV = \frac{\frac{dT}{dt}}{\frac{dV}{dt}} = \frac{dT}{dV} \tag{10}$$

where dT denotes the difference in cell temperature and dV denotes the difference in voltage. The DTV analysis commenced with the data preprocessing procedures outlined in Section (1). Illustrations in Figure 2(a) and Figure 2(c) depict the evolution of the DTV curve with battery aging. For both datasets, which vary in cell composition and operational environments, the curves exhibit two prominent peaks and a single trough.

4) Correlation analysis and its feature selection: In this research, we concentrate on extracting features from the Differential Thermal Voltage (DTV) and Incremental Capacity (IC) curves of lithium-ion batteries. Our feature extraction framework highlights how DTV and IC curve characteristics evolve with battery degradation. Notably, the peaks and troughs on these curves undergo significant changes as the battery ages, with DTV curve peaks and troughs shifting towards higher voltages, and similarly, IC curve peaks and troughs also moving towards higher voltages. These shifts are closely linked to the aging process of the battery. Typically, the extracted features include the magnitude and position of the DTV and IC curve peaks and troughs. More precisely, we initially identify the first peak of the DTV curve and its associated voltage, along with the first peak of the IC curve and its corresponding voltage as key features. Additionally, this study employs the LLE technique for feature extraction. We then conduct a comparative analysis between the peak

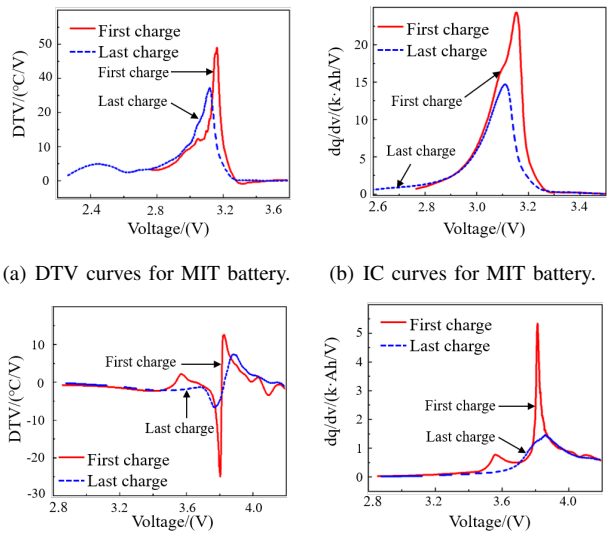

(a) DTV curves for MIT battery. (b) IC curves for MIT battery.

(c) DTV curves for Oxford battery. (d) IC curves for Oxford battery.

Fig. 2: Schematic of feature extraction.

and trough features and the dimensionality-reduced DTV and IC features obtained through LLE. The Pearson correlation coefficient is utilized to assess the relationship between these features and battery capacity, calculated as follows:

$$r_{xy} = \frac{\sum_{i=1}^{n}(x_i - \bar{x})(y_i - \bar{y})}{\sqrt{\sum_{i=1}^{n}(x_i - \bar{x})^2}\sqrt{\sum_{i=1}^{n}(y_i - \bar{y})^2}} \tag{11}$$

The outcomes of the correlation analysis are presented in Table III and Table IV, and the description of each variable is shown in Table II. Traditionally, extracting features from peaks and troughs involves extensive data preprocessing, including filtering, noise reduction, and eliminating disturbances to secure high-quality data for reliable feature extraction. These steps aim to precisely determine the location and intensity of peaks and troughs, thereby capturing critical data variations. In contrast, the LLE approach streamlines the feature extraction process, bypassing the need for complex preprocessing while still identifying features that have a strong correlation with the data. The correlation coefficients obtained through LLE surpass those achieved by conventional methods of peak and trough extraction. Moreover, LLE offers greater computational efficiency, enabling quicker completion of the feature extraction phase. Overall, the LLE technique demonstrates clear superiority in extracting features.

TABLE II: DESCRIPTION OF FEATURES

Feature	Description
A	The first peak of the DTV curve
B	Voltage when the DTV curve at first peak
C	The first peak of the IC curve
D	Voltage when the IC curve at first peak
E	The dimensionality-reduced DTV
E	The dimensionality-reduced IC

III. METHODOLOGY

The methodology proposed in this study is illustrated in Figure 3. In this methodology, the TimeGAN algorithm

TABLE III: CORRELATION ANALYSIS BETWEEN BATTERY CAPACITY AND VARIOUS FEATURES OF MIT BATTERIES

Feature	#20	#22	#36	#44
A	0.968	0.976	0.973	0.977
B	0.971	0.982	0.985	0.989
C	0.968	0.976	0.974	0.979
D	0.975	0.985	0.988	0.985
E	0.998	0.996	0.990	0.993
F	0.997	0.995	0.995	0.992

TABLE IV: CORRELATION ANALYSIS BETWEEN BATTERY CAPACITY AND VARIOUS FEATURES OF OXFORD BATTERIES

Feature	#1	#3	#4	#7	#8
A	0.980	0.964	0.967	0.942	0.974
B	0.956	0.961	0.956	0.961	0.926
C	0.955	0.957	0.970	0.963	0.979
D	0.979	0.978	0.983	0.986	0.972
E	0.990	0.993	0.992	0.994	0.987
F	0.988	0.990	0.991	0.990	0.982

plays a pivotal role during the training phase by generating additional data to reflect patterns present in the battery capacity degradation data. Subsequently, this augmented dataset is utilized to enhance the model's ability to recognize patterns in unseen data, culminating in the utilization of a fusion prediction structure to train the predictive model. Prior to training, the data is partitioned in a 3:7 ratio, with 30% of the data used for testing residual life prediction, while the remaining 70% undergoes data augmentation using TimeGAN before training commences. The MIT dataset, which employs a lithium iron phosphate battery system, is a part of this study and contrasts with the ternary system used in the Oxford dataset. This disparity allows for the evaluation of the proposed methodology's accuracy and generalization capabilities across different types of battery materials. Through the application of these datasets, this study aims to comprehensively evaluate the performance of the proposed methodology across various material systems.

A. *Pyraformer Network Model*

1) Model Architecture: The Pyraformer employs a pyramidal attention mechanism within its neural network framework, as depicted in Figure 4. Initially, it adopts a data preprocessing technique akin to that used in the Informer model, where observations, covariates, and spatial data are embedded independently before being aggregated, mirroring the approach of the Transformer. Subsequently, it constructs a multi-resolution C-ary tree through the Coarse Scale Construction Module (CSCM), where each coarse-scale node encapsulates the data from its finer-scale C counterparts. To adeptly handle varying temporal dependencies, the model integrates the Pyramid Attention Module (PAM). This module leverages a pyramid-shaped attention graph to facilitate information flow. The model then tailors its network architecture to suit specific downstream tasks, culminating in the generation of predictive outcomes.

2) Position coding: Positional encoding assigns distinct codes to each position vector in a sequence through varying frequencies of sine and cosine functions. This technique

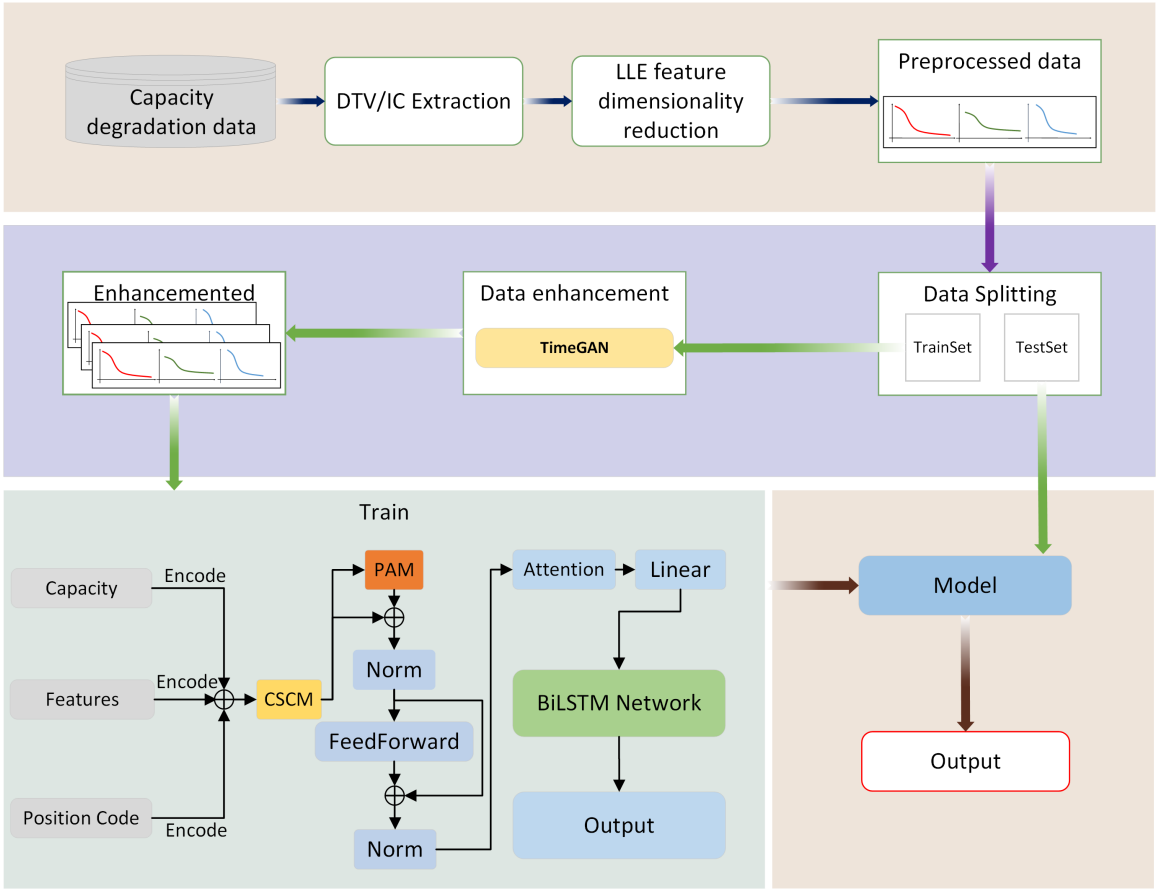

Fig. 3: Overall Design of TimeGAN-Pyraformer-BiLSTM Model

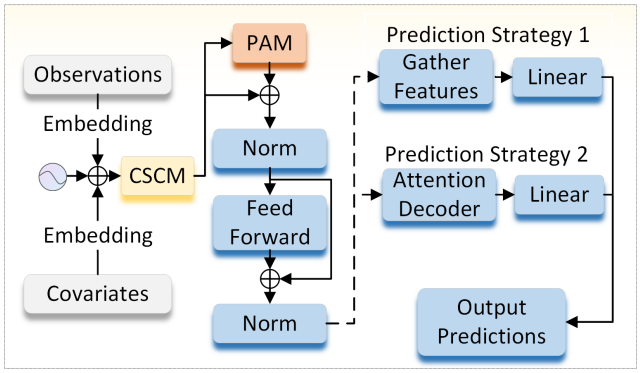

Fig. 4: Pyraformer Network Structure

enables the model to understand the order of elements within the sequence, essential for handling tasks that depend on temporal data.

$$PE(t, 2k) = \sin\left(\frac{t}{10000^{2k/s}}\right) \tag{12}$$

$$PE(t, 2k+1) = \cos\left(\frac{t}{10000^{2k/s}}\right) \tag{13}$$

In this context, PE signifies the matrix used for position encoding, with s representing the dimensionality of each position vector within the model. The variable t indicates the specific position of an item within the sequence, while k is an integer ranging from 0 to (s/2-1), serving as the dimension index for the encoded vector.

3) Multi-Scale Pyramidal Attention Structure: The Pyraformer incorporates the Pyramidal Attention Module (PAM) to understand temporal relationships over diverse spans, illustrated in Figure 5(a). Utilizing a hierarchical tree architecture, this module conducts self-attention processes, facilitating the extraction of multi-resolution features via connections between different scales. Additionally, connections within the same scale are used to depict the interdependencies among various resolutions. Within the pyramidal

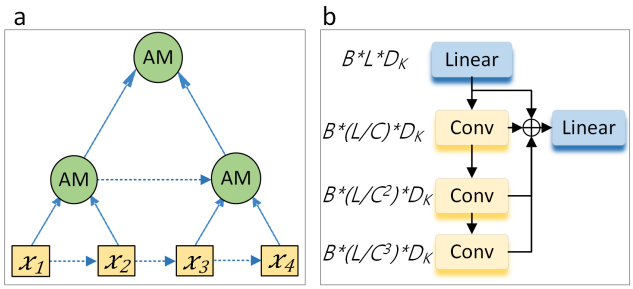

Fig. 5: PAM and CSCM

graph framework, nodes at the lowest level correspond to individual observations over time, whereas nodes at higher levels are tasked with aggregating and extracting features from their subordinate nodes. This structure enables the identification of node relationships at each tier. Upper-level nodes, which assimilate information from nodes below and engage in feature extraction across extended time frames, necessitate only the examination of connections between

neighboring nodes on the same level, thereby simplifying the computational demands. The pyramidal graph design of the Pyraformer thus efficiently captures temporal dependencies within the sequence through a multi-resolution approach.

4) Coarse-Scale Construction Module (CSCM): The Coarse-Scale Construction Module (CSCM) compiles the embedded sequences across various scales, forming a multi-resolution tree architecture that facilitates effective communication among nodes via the PAM. By sequentially adding coarse-scale nodes from the lower levels upwards, the CSCM achieves this through convolution operations on the respective child nodes,C^S (C is a constant; S is the number of convolutional layers the sequence passes through; $S = 0, 1, 2$).

In the time dimension, multiple convolutional layers with a kernel size of C and a stride of C are applied sequentially to the embedded sequence, thereby generating sequences of length $L/C^S + 1$ (where L is the length of the input sequence). These sequences, ranging from fine to coarse, are concatenated and fed into the PAM. To reduce the number of parameters and computational load, each node is dimensionally reduced through a fully connected layer before being input into the cascading convolutional layers, and the original dimensionality is restored after all convolutions. Such a structure significantly reduces the number of parameters in the module and can prevent overfitting. The module structure is shown in Figure 5(b), where B is the batch size; D is the feature dimension of each node; D_K is the feature dimension of the key vector.

B. BiLSTM Module

BiLSTM is composed of a pair of LSTM networks that process temporal data in both forward and reverse directions. In this architecture, the output vectors from each direction are merged into a single vector, providing a comprehensive representation of the sequence at hand. This allows BiLSTM to effectively harness information from both past and future contexts, offering a more nuanced understanding of temporal dynamics within the data compared to a standard LSTM.

$$f_t = \text{sigmoid}(W_{fx}x_t + W_{fs}s_{t-1} + b_t) \tag{14}$$

$$i_t = \text{sigmoid}(W_{ix}x_t + W_{is}s_{t-1} + b_i) \tag{15}$$

$$\tilde{c}_t = \tan(W_{cx}x_t + W_{cs}s_{t-1} + b_c) \tag{16}$$

$$o_t = \text{sigmoid}(W_{ox}x_t + W_{os}s_{t-1} + b_c) \tag{17}$$

$$c_t = \tan(c_t) \tag{18}$$

Where f_t is the output of the forget gate, which is the output signal of the output gate, i_t is the preliminary information to be input into the memory cell, o_t is the output signal of the output gate, and $\tilde{c}_t$ is the preliminary information to be output to the hidden layer state s.

C. Time-series Generative Adversarial Networks

TimeGAN, a novel approach for synthesizing time series data, combines the unsupervised learning capabilities of Generative Adversarial Networks (GANs) with the predictive precision of supervised autoregressive models to effectively manage the dynamics of time-dependent data. It incorporates a supervised loss alongside a concurrently trained embedding network to markedly improve the fidelity of the generated time series. TimeGAN is structured around four principal components: an embedding mechanism, a recovery mechanism, a generator for sequences, and a discriminator for sequences. Its distinctive feature is the integrated training of both the autoencoder components (embedding and recovery mechanisms) and the adversarial components (sequence generator and discriminator), enabling the model to adeptly encode time series features, generate accurate representations, and navigate through temporal sequences.

D. Fusion Prediction Structure

This study introduces a hybrid forecasting framework that leverages the Pyraformer model's proficiency in handling extended sequences alongside the BiLSTM model's adeptness at maintaining time series continuity. The proposed framework encompasses both direct and recursive prediction mechanisms. The direct prediction segment is tasked with projecting future values for the entire time series, offering a macroscopic view of the trend over the forecast period. Conversely, the recursive prediction component utilizes outcomes from the preceding step (incorporating both Pyraformer and prior BiLSTM predictions) to sequentially forecast subsequent points. This approach enables the detection of finer time series nuances, particularly short-term variations that may not be fully captured by Pyraformer alone. The underlying principle of model prediction is outlined as follows:

$$\hat{X}_{\text{direct}}^{(t+1)}, \ldots, \hat{X}_{\text{direct}}^{(t+m)} = f_{\text{Pyraformer}}\left(X^{(t-n)}, \ldots, X^{(t)}\right) \tag{19}$$

$$\begin{aligned} \hat{X}_{\text{recursive}}^{(t+1)} &= f_{\text{BiLSTM}}\left(X^{(t-n+1)}, \ldots, \hat{X}_{\text{direct}}^{(t+1)}\right), \\ \hat{X}_{\text{recursive}}^{(t+2)} &= f_{\text{BiLSTM}}\left(X^{(t-n+2)}, \ldots, \hat{X}_{\text{direct}}^{(t+2)}\right), \\ &\vdots \\ \hat{X}_{\text{recursive}}^{(t+m)} &= f_{\text{BiLSTM}}\left(\hat{X}_{\text{direct}}^{(t+1)}, \ldots, \hat{X}_{\text{direct}}^{(t+m)}\right) \end{aligned} \tag{20}$$

Where $X = [\text{capacity}, \text{feature1}, \text{feature2}]$ represents the capacity value and multiple feature variables at a time point, $\hat{X}_{\text{direct}}$ is the capacity value and multiple feature variables at a time point predicted by the Pyraformer model, and $\hat{X}_{\text{recursive}}$ is the final prediction result iteratively predicted by the BiLSTM model based on the predictions of the Pyraformer model.

IV. Validation and Results Analysis

Following the outlined testing methodology, experiments were conducted on the proposed model as follows: Initially, historical battery capacity data designated for prediction was input into the model. The model then forecasted the capacity for the next time step, with the prediction error calculated

by comparing it to the actual capacity. This predicted value was integrated into the test dataset for the next prediction cycle, a process that continued until the forecasted capacity dropped below the specified capacity threshold. The count of these prediction cycles was noted as the estimated Remaining Useful Life (RUL), which was then evaluated against the true RUL. Evaluation of the model's performance utilized the cumulative error from single-step forecasts and the total error in RUL estimation as key metrics. For fairness in comparison, identical training configurations were applied across all models. The model's loss was determined using MAE, with optimization carried out via the Adam optimizer. A learning rate of 0.001 and a training duration of 100 epochs were set. The length of the capacity vector inputted into the model ranged from 5% to 10% of the entire dataset's length, equivalent to 64 for the MIT dataset and 5 for the Oxford dataset. The experimental results were generated using a system equipped with a 12th Gen Intel® Core™ i5-12490F CPU at 2.50GHz, 16GB RAM, an NVIDIA GeForce RTX 3070 GPU with 8GB cache, Python 3.7, and PyTorch 1.8.0. Detailed experimental findings are provided below.

A. Evaluation Metrics

RUL of a battery is defined as the count of charge-discharge cycles it can undergo before its capacity falls below a predetermined failure threshold under existing conditions. In this study, the open-source dataset utilized records various parameters at uniform intervals throughout the charge-discharge cycles. This leads to a broad spectrum and extended intervals in the recorded numbers of the final charge-discharge cycles. Consequently, this research interprets the data sampling points' sequence numbers within the total sampling sequence as an indicator of battery life. The period until the capacity diminishes to below the failure threshold at a specific point in time is regarded as the battery's remaining life.

$$RUL = \text{Index}_{\text{EOL}} - \text{Index}_{\text{now}} \tag{21}$$

This paper sets the battery failure threshold at 80% of its rated capacity. It assesses the effectiveness of a full iterative prediction on remaining life by comparing predicted charge-discharge cycles with actual ones. The error in final cycle prediction is quantified using Cycle Absolute Error (CAE).

$$CAE = RUL_{\text{predict}} - RUL_{\text{true}} \tag{22}$$

Where RUL_{predict} represents the predicted value of remaining charge-discharge cycles, and RUL_{true} represents the actual value of remaining charge-discharge cycles.

This paper employs Mean Absolute Error (MAE) and Root Mean Square Error (RMSE) to analyze capacity prediction errors in single-step predictions.

$$MAE = \frac{1}{n}\sum_{i=1}^{n}|y_i - \hat{y}_i| \tag{23}$$

$$RMSE = \sqrt{\frac{1}{n}\sum_{i=1}^{n}(y_i - \hat{y}_i)^2} \tag{24}$$

In the aforementioned formulas, N represents the total number of samples in the dataset involved in the evaluation; y_i represents the actual value of the battery capacity in the dataset; $\hat{y}_i$ represents the predicted battery capacity value; $\bar{y}_i$ represents the average actual capacity value. MAE and $RMSE$ represent the error between the predicted values and the actual values, so the smaller the value, the better the model performance.

B. Analysis of Experimental Results

Building upon the prediction method and evaluation metrics introduced earlier, this paper conducted a series of experiments comparing several traditional recurrent neural networks and documented the results. For the test battery samples, we utilized 30% and 40% of the complete battery dataset as prediction starting points. Autoregressive prediction was employed to evaluate the accuracy of the model in life prediction and confirm its effectiveness.

Figure 6 to Figure 9 show the prediction comparison results for the MIT and Oxford dataset. Each graph represents a different training split ratio. Each line in the figure corresponds to a different cell, with a thumbnail on the left and a detailed view of the prediction near the capacity termination line on the right. In the prediction results, each line represents a network model, and the red vertical dashed line indicates the starting point of the prediction. The gray horizontal dashed line represents 80% of the original capacity, and the intersection of this line with the dashed line on the Y-coordinate indicates the failure cycle of the battery.

The figures demonstrate that the prediction method proposed in this paper generates capacity degradation curves closest to the actual capacity values compared to other methods. The predicted battery cycle life varies notably across different training ratios, highlighting the effectiveness and adaptability of our approach across various stages of battery degradation. In contrast, other methods display larger errors relative to actual values.

This paper also presents a visualization comparing recursively predicted remaining life with actual remaining life to assess the model's accuracy in predicting remaining life. Figure 10 display this comparison. Comparisons reveal that the proposed prediction method in this paper achieves significantly higher accuracy than other basic recurrent neural networks on the MIT battery data. Although on the Oxford battery dataset, where battery capacity sampling is sparser and the range of charge-discharge cycles is smaller, the advantage of our method isn't as apparent, our method still outperforms others in most predictions, demonstrating good stability.

Based on experimental results, this paper utilizes MAE and RMSE as evaluation metrics to calculate prediction errors of various models on two battery datasets, as displayed in Tables V to VIII. Taking MIT #20 battery as an example, when predict start at 30% of data, our method achieves MAE error of 1.56% and RMSE error of 2.03%, improving 52.87% and 53.97% respectively compared to the sub-optimal algorithm. At 40% training set ratio, MAE error reduces to 0.83% and RMSE error to 1.01%, improving 79.20% and 84.36% respectively. Similar improvements are observed for Oxford batteries. These results demonstrate not only smaller error values across different training set ratios and battery types but also excellent generalization ability, crucial for battery health management. The method maintains prediction accuracy across diverse datasets and usage conditions,

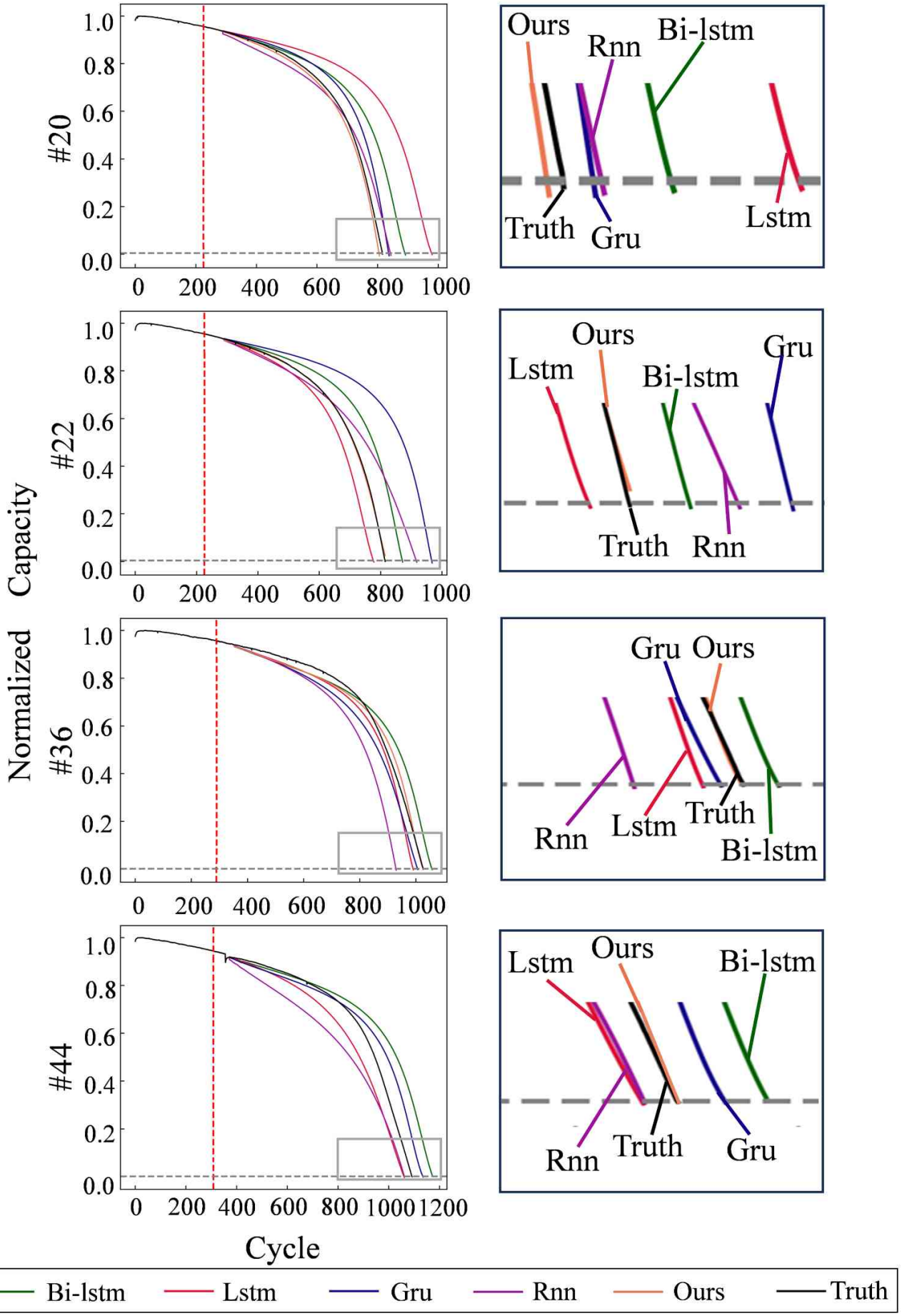

Fig. 6: The predict results of different batteries on MIT dataset when predict start at 30%. Thumbnails on the left and details on the right.

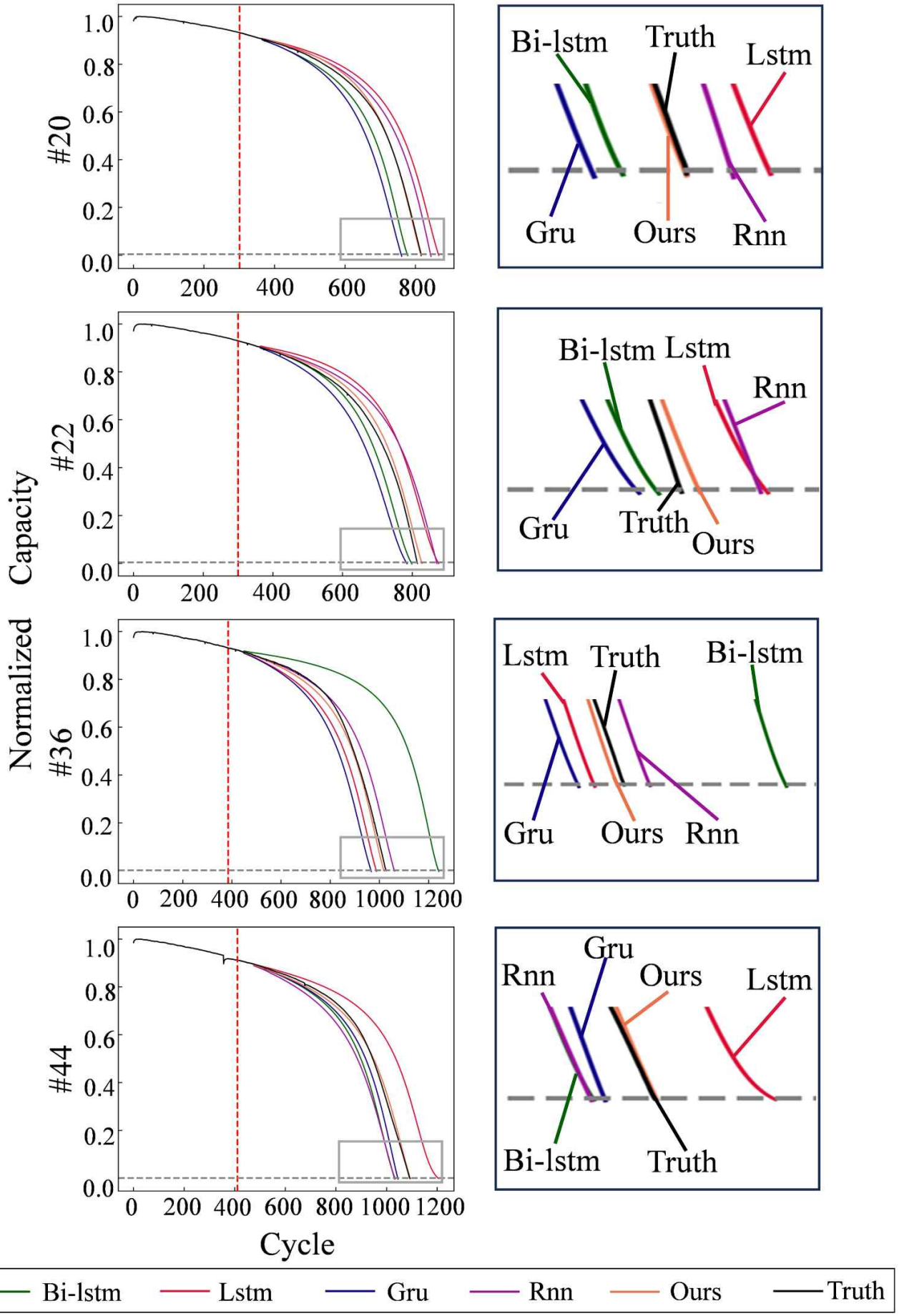

Fig. 7: The predict results of different batteries on MIT dataset when predict start at 40%. Thumbnails on the left and details on the right.

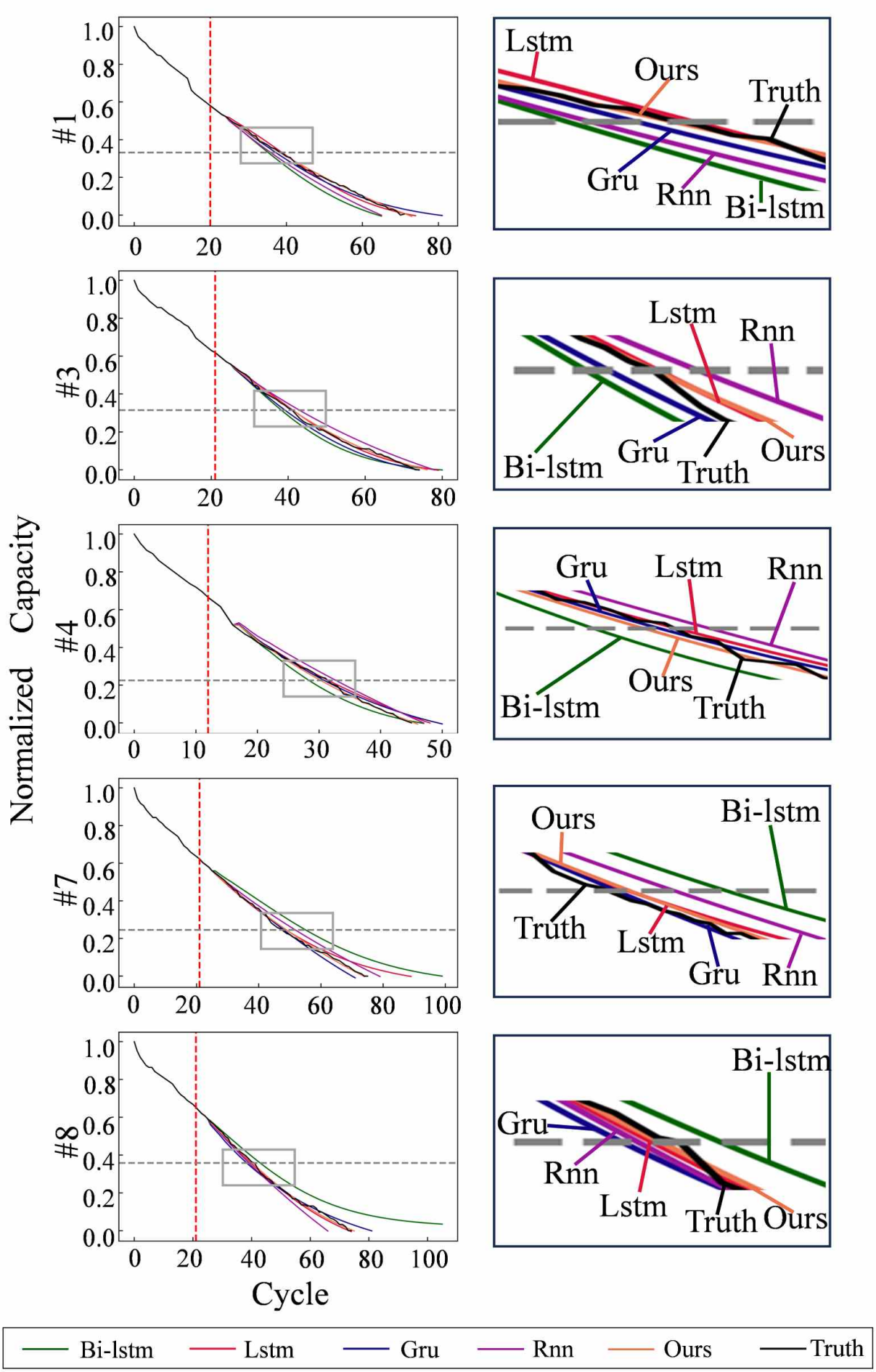

Fig. 8: The predict results of different batteries on Oxford dataset when predict start at 30%. Thumbnails on the left and details on the right.

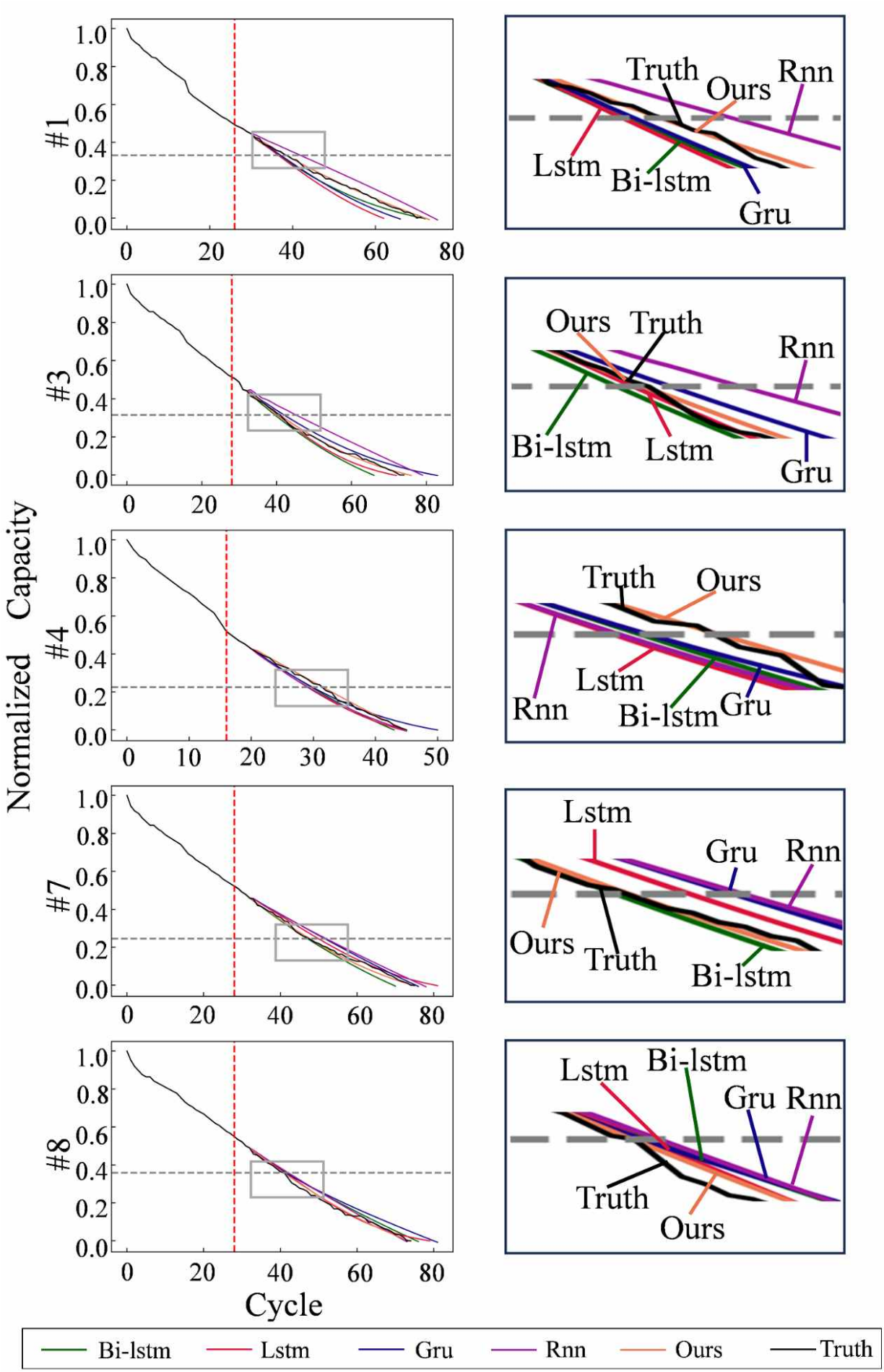

Fig. 9: The predict results of different batteries on Oxford dataset when predict start at 40%. Thumbnails on the left and details on the right.

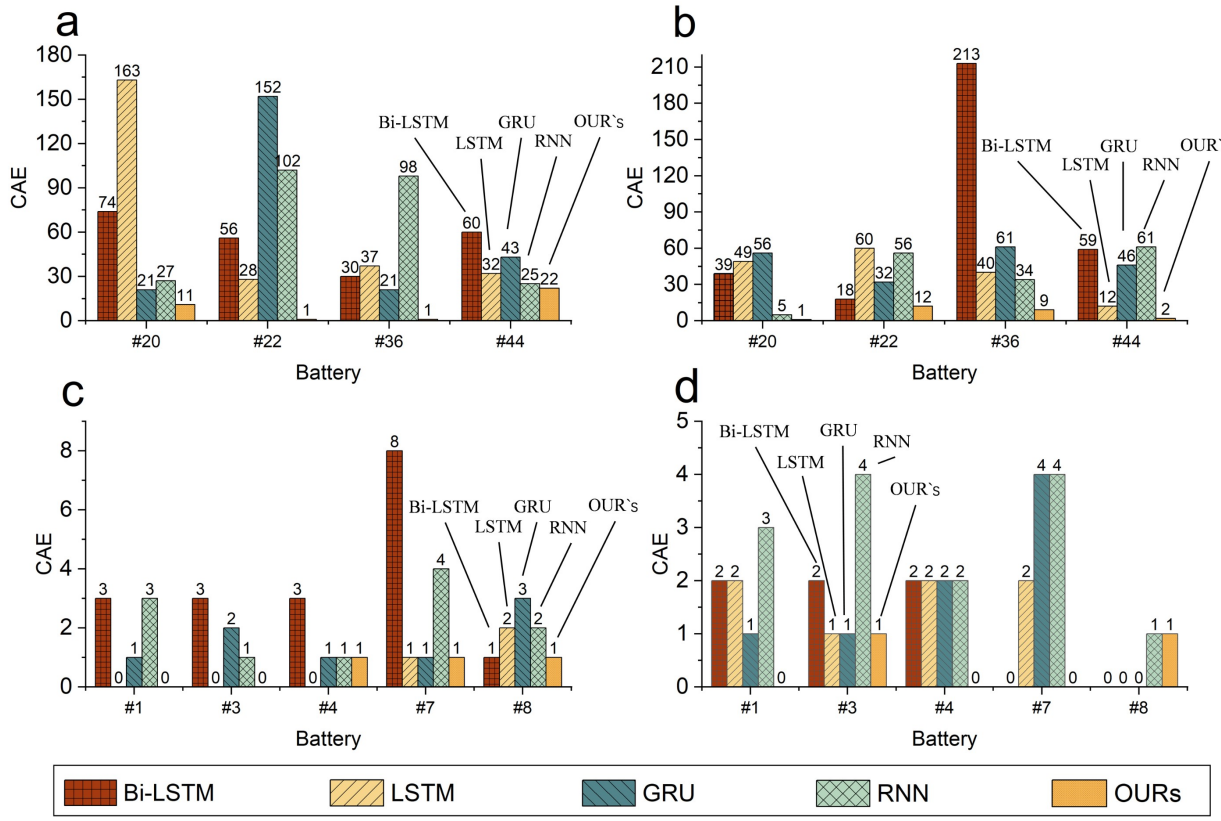

Fig. 10: Error analysis of the prediction results.(a) predict start at 30% on MIT batteries. (b) predict start at 40% on MIT batteries. (c) predict start at 30% on Oxford batteries. (d) predict start at 40% on Oxford batteries.

TABLE V: ERROR ANALYSIS FOR MIT BATTERIES WHEN PREDICT START AT 30%.

	#20		#22		#36		#44	
Model	MAE	RMSE	MAE	RMSE	MAE	RMSE	MAE	RMSE
Bi-LSTM	7.09	12.49	6.99	11.32	4.52	6.64	6.52	11.82
LSTM	11.89	19.53	5.75	9.10	3.56	4.62	6.49	8.25
GRU	4.89	7.26	12.44	20.07	5.37	6.24	4.44	7.30
RNN	3.31	4.41	4.70	8.64	9.38	13.41	11.01	12.40
OUR	**1.56**	**2.03**	**0.36**	**0.53**	**2.41**	**2.80**	**2.24**	**2.43**

TABLE VI: ERROR ANALYSIS FOR MIT BATTERIES WHEN PREDICT START AT 40%.

	#20		#22		#36		#44	
Model	MAE	RMSE	MAE	RMSE	MAE	RMSE	MAE	RMSE
Bi-LSTM	5.84	9.01	4.02	6.80	15.32	24.10	5.93	8.84
LSTM	6.34	9.77	7.39	10.24	6.25	8.18	8.37	13.49
GRU	8.40	12.89	7.87	11.40	9.00	12.29	3.95	5.72
RNN	4.01	6.47	6.28	9.90	3.21	5.84	7.53	10.09
OUR	**0.83**	**1.01**	**2.01**	**2.62**	**1.64**	**2.03**	**1.13**	**1.41**

showcasing practicality and reliability in battery performance prediction. Its strong generalization enables adaptation to new battery types and scenarios, serving as a valuable tool for battery management system development, contributing to extending battery life, enhancing energy efficiency, and cutting maintenance costs. These traits render our method not only academically significant but also highly practical for industrial applications.

V. Conclusion

This study introduces a novel method for predicting the Remaining Useful Life (RUL) of lithium-ion batteries, leveraging a combination of TimeGAN for data augmentation, Pyraformer for long sequence prediction, and BiLSTM for recursive single-step prediction. The synergy among these components provides our method with a notable edge in RUL prediction for lithium-ion batteries. Our method, along with traditional RNN and LSTM models, was subjected to experimental validation using both the Oxford and MIT open-source battery datasets. The findings demonstrate a

TABLE VII: ERROR ANALYSIS FOR OXFORD BATTERIES WHEN PREDICT START AT 30%.

	#1		#3		#4		#7		#8	
Model	MAE	RMSE	MAE	RMSE	MAE	RMSE	MAE	RMSE	MAE	RMSE
Bi-LSTM	4.78	5.47	2.79	3.24	2.49	3.17	5.73	6.41	4.54	5.41
LSTM	1.21	1.51	0.83	1.08	1.46	1.89	1.53	2.01	1.02	1.32
GRU	1.17	1.42	1.79	2.10	1.29	1.68	1.27	1.88	1.46	1.88
RNN	3.39	3.84	2.54	2.93	2.71	3.00	2.64	3.11	2.54	3.39
OUR	**0.42**	**0.62**	**0.74**	**0.94**	**0.83**	**1.12**	**0.73**	**0.93**	**0.69**	**0.92**

TABLE VIII: ERROR ANALYSIS FOR OXFORD BATTERIES WHEN PREDICT START AT 40%.

	#1		#3		#4		#7		#8	
Model	MAE	RMSE	MAE	RMSE	MAE	RMSE	MAE	RMSE	MAE	RMSE
Bi-LSTM	2.31	2.71	2.74	3.50	1.84	2.20	1.88	2.50	2.13	2.53
LSTM	4.47	5.44	1.89	2.40	2.24	2.70	1.51	1.84	1.19	1.44
GRU	3.13	3.76	2.14	2.41	1.34	1.72	2.29	2.76	3.04	3.55
RNN	3.95	4.35	5.06	5.56	1.89	2.34	2.86	3.24	1.94	2.46
OUR	**0.48**	**0.64**	**0.61**	**0.83**	**0.65**	**0.92**	**0.86**	**1.13**	**1.04**	**1.25**

significant improvement in prediction performance compared to other approaches. Our proposed network model presents evident benefits in terms of precision and dependability. Its extensive applicability aids in boosting battery management efficiency and sustainability, thereby fostering the progress of battery technology. Future studies might delve deeper into refining and exploring this approach to tackle more intricate battery systems and diverse application scenarios.

REFERENCES

[1] H. Chaoui and C. C. Ibe-Ekeocha, "State of charge and state of health estimation for lithium batteries using recurrent neural networks," *IEEE Transactions on vehicular technology*, vol. 66, no. 10, pp. 8773–8783, 2017.

[2] Z. Jiang, H. Li, Z. Qu, and J. Zhang, "Recent progress in lithium-ion battery thermal management for a wide range of temperature and abuse conditions," *International journal of hydrogen energy*, vol. 47, no. 15, pp. 9428–9459, 2022.

[3] Z. Jiang and Z. Qu, "Lattice boltzmann simulation of ion and electron transport in lithium ion battery porous electrode during discharge process," *Energy Procedia*, vol. 88, pp. 642–646, 2016.

[4] Z. Jiang, Z. Qu, L. Zhou, and W. Tao, "A microscopic investigation of ion and electron transport in lithium-ion battery porous electrodes using the lattice boltzmann method," *Applied energy*, vol. 194, pp. 530–539, 2017.

[5] Y. Hua, X. Liu, S. Zhou, Y. Huang, H. Ling, and S. Yang, "Toward sustainable reuse of retired lithium-ion batteries from electric vehicles," *Resources, Conservation and Recycling*, vol. 168, p. 105249, 2021.

[6] J. Lin, X. Liu, S. Li, C. Zhang, and S. Yang, "A review on recent progress, challenges and perspective of battery thermal management system," *International Journal of Heat and Mass Transfer*, vol. 167, p. 120834, 2021.

[7] J. Mou, P. Duan, L. Gao, X. Liu, and J. Li, "An effective hybrid collaborative algorithm for energy-efficient distributed permutation flow-shop inverse scheduling," *Future Generation Computer Systems*, vol. 128, pp. 521–537, 2022.

[8] D. Gao and M. Huang, "Prediction of remaining useful life of lithium-ion battery based on multi-kernel support vector machine with particle swarm optimization," *Journal of Power Electronics*, vol. 17, no. 5, pp. 1288–1297, 2017.

[9] J. Li, D. Wang, L. Deng, Z. Cui, C. Lyu, L. Wang, and M. Pecht, "Aging modes analysis and physical parameter identification based on a simplified electrochemical model for lithium-ion batteries," *Journal of Energy Storage*, vol. 31, p. 101538, 2020.

[10] L. Ma, Y. Xu, H. Zhang, F. Yang, X. Wang, and C. Li, "Co-estimation of state of charge and state of health for lithium-ion batteries based on fractional-order model with multi-innovations unscented kalman filter method," *Journal of Energy Storage*, vol. 52, p. 104904, 2022.

[11] L. Fan, X. Lu, Y. Liu, and Q. Xu, "Remaining useful life prediction of lithium-ion battery based on data-driven and multi-model fusion," SAE Technical Paper, Tech. Rep., 2022.

[12] K. K. Sadabadi, X. Jin, and G. Rizzoni, "Prediction of remaining useful life for a composite electrode lithium ion battery cell using an electrochemical model to estimate the state of health," *Journal of Power Sources*, vol. 481, p. 228861, 2021.

[13] C. JI, J.-z. WANG, and R. GENG, "Weak-selection backtracking matching pursuit algorithm based on dice coefficient," *Journal of Northeastern University (Natural Science)*, vol. 42, no. 2, p. 189, 2021.

[14] J. Meng, T. Azib, and M. Yue, "Early-stage end-of-life prediction of lithium-ion battery using empirical mode decomposition and particle filter," *Proceedings of the Institution of Mechanical Engineers, Part A: Journal of Power and Energy*, vol. 237, no. 5, pp. 1090–1099, 2023.

[15] P. Singh, C. Chen, C. M. Tan, and S.-C. Huang, "Semi-empirical capacity fading model for soh estimation of li-ion batteries," *Applied Sciences*, vol. 9, no. 15, p. 3012, 2019.

[16] S. Rahimifard, S. Habibi, G. Goward, and J. Tjong, "Adaptive smooth variable structure filter strategy for state estimation of electric vehicle batteries," *Energies*, vol. 14, no. 24, p. 8560, 2021.

[17] B. Yang, D. Wang, B. Zhang, S. Chen, X. Sun, and T. Wang, "Aging diagnosis-oriented three-scale impedance model of lithium-ion battery inspired by and reflecting morphological evolution," *Journal of Energy Storage*, vol. 59, p. 106357, 2023.

[18] F. Guan, T. Wang, S. Wang, H. Zhang, and H. Men, "Soc estimation of lithium battery based on abc-rfekf algorithm," *Power System Protection and Control*, vol. 50, no. 4, pp. 163–171, 2022.

[19] F. Na, C. Hao, D. Xin, and X. Wei, "Short-term power load forecasting based on vmd-arima-dbn," in *Proceedings of the CSU-EPSA*, vol. 35, no. 6, 2023, pp. 59–65.

[20] D. JIAN, P. LI, and Y. HUANG, "Short-term power load forecasting based on ga-vmd-resnet-lstm network," *Foreign Electronic Measurement Technology*, vol. 41, no. 10, pp. 15–22, 2022.

[21] B. Deng, N. Zhang, J. Wang, and L. Ge, "Medium-and long-term power load forecasting method based on ltc-rnn model," *Journal of Tianjin University (Science and Technology)*, vol. 55, no. 10, pp. 1026–1033, 2022.

[22] Y. Junqi, N. Jikai, Z. Anjun, and H. Xueyan, "Arima-gru short-term power load forecasting based on feature mining [j]," *Journal of Electric Power Systems and Automation*, vol. 34, no. 3, p. 9, 2022.

[23] W. Zhang, C. Yu, S. Wang, T. Li, X. He, and J. Chen, "Multifeatured short-term power load forecasting based on vmd-lstm-lightgbm," *Southern Grid Technology*, vol. 17, pp. 74–81, 2023.

[24] M. Morchid, "Parsimonious memory unit for recurrent neural networks with application to natural language processing," *Neurocomputing*, vol. 314, pp. 48–64, 2018.

[25] A. Vaswani, N. Shazeer, N. Parmar, J. Uszkoreit, L. Jones, A. N. Gomez, Ł. Kaiser, and I. Polosukhin, "Attention is all you need," *Advances in neural information processing systems*, vol. 30, 2017.

[26] S. Liu, H. Yu, C. Liao, J. Li, W. Lin, A. X. Liu, and S. Dustdar, "Pyraformer: Low-complexity pyramidal attention for long-range time series modeling and forecasting," in *International conference on learning representations*, 2021.

[27] Y. Zhou, H. Gu, T. Su, X. Han, L. Lu, and Y. Zheng, "Remaining useful life prediction with probability distribution for lithium-ion batteries based on edge and cloud collaborative computation," *Journal of Energy Storage*, vol. 44, p. 103342, 2021.
[28] Z. Wang, N. Liu, C. Chen, and Y. Guo, "Adaptive self-attention lstm for rul prediction of lithium-ion batteries," *Information Sciences*, vol. 635, pp. 398–413, 2023.
[29] Z. Zhang, H. Min, H. Guo, Y. Yu, W. Sun, J. Jiang, and H. Zhao, "State of health estimation method for lithium-ion batteries using incremental capacity and long short-term memory network," *Journal of Energy Storage*, vol. 64, p. 107063, 2023.
[30] H. Meng, M. Geng, and T. Han, "Long short-term memory network with bayesian optimization for health prognostics of lithium-ion batteries based on partial incremental capacity analysis," *Reliability Engineering & System Safety*, vol. 236, p. 109288, 2023.
[31] M. Lin, C. Yan, W. Wang, G. Dong, J. Meng, and J. Wu, "A data-driven approach for estimating state-of-health of lithium-ion batteries considering internal resistance," *Energy*, vol. 277, p. 127675, 2023.
[32] S. Shao, P. Wang, and R. Yan, "Generative adversarial networks for data augmentation in machine fault diagnosis," *Computers in Industry*, vol. 106, pp. 85–93, 2019.
[33] I. Goodfellow, J. Pouget-Abadie, M. Mirza, B. Xu, D. Warde-Farley, S. Ozair, A. Courville, and Y. Bengio, "Generative adversarial nets," *Advances in neural information processing systems*, vol. 27, 2014.
[34] M. Mirza and S. Osindero, "Conditional generative adversarial nets," *arXiv preprint arXiv:1411.1784*, 2014.
[35] J. Yoon, D. Jarrett, and M. Van der Schaar, "Time-series generative adversarial networks," *Advances in neural information processing systems*, vol. 32, 2019.
[36] K. A. Severson, P. M. Attia, N. Jin, N. Perkins, B. Jiang, Z. Yang, M. H. Chen, M. Aykol, P. K. Herring, D. Fraggedakis *et al.*, "Data-driven prediction of battery cycle life before capacity degradation," *Nature Energy*, vol. 4, no. 5, pp. 383–391, 2019.
[37] C. Birkl, "Diagnosis and prognosis of degradation in lithium-ion batteries," Ph.D. dissertation, University of Oxford, 2017.

Xiaoxin Li(M'24) is a postgraduate student at the Software College, Liaoning Technical University, Huludao, China. She became a Member (M) of IAENG in 2024. Her research interests include: data-driven traffic simulation and intelligent transportation system.

Qiang Ai(M'24) is currently a postgraduate student at the School of Computer, Qinghai Normal University, Xining, China. He received his bachelor's degree from Software College, Liaoning Technical University. He became a Member (M) of IAENG in 2024. He has been worked at the Institute of Information Engineering, Chinese Academy of Sciences. His research interests include: spatial-temporal big data, knowledge graph and intelligent transportation system.

Ming Xu received his Ph.D. degree in computer science from Beijing University of Posts and Telecommunications, Beijing, China, in 2015. From 2016 to 2019, he was a Post-Doctoral Fellow with Tsinghua University, Beijing, China. He is currently a professor at the Software College, Liaoning Technical University. He has published over 20 papers in journals and conferences, including TITS, BIBM and TCSS. His research work has reported by MIT Technology Reviews. He is the recipient of "the 2020 World Artificial Intelligence Conference Youth Outstanding Paper" (WAICYOP) award. His research interests include: graph learning, spatio-temporal data mining, reinforcement learning and data-driven traffic simulation